Petroleum Science 22 (2025) 3803–3816

Contents lists available at ScienceDirect

Petroleum Science

journal homepage: www.keaipublishing.com/en/journals/petroleum-science

Original Paper

Deep feature learning for anomaly detection in gas well deliquification using plunger lift: A novel CNN-based approach

Qi-Xin Liu [a], Jian-Jun Zhu [a,*], Hai-Bo Wang [e], Shuo Chen [a], Hao-Yu Wang [b], Nan Li [b], Rui-Zhi Zhong [c], Yu-Jun Liu [a], Hai-Wen Zhu [d,**]

[a] College of Mechanical and Transportation Engineering, China University of Petroleum (Beijing), Beijing, 102249, China
[b] PetroChina Research Institute of Petroleum Exploration & Development, Beijing, 100083, China
[c] Centre for Natural Gas, The University of Queensland, Brisbane, QLD, 4072, Australia
[d] McDougall School of Petroleum Engineering, The University of Tulsa, 800 S Tucker Dr, Tulsa, OK, 74104, USA
[e] PetroChina Tuha Oilfield Company, Hami, 839009, Xinjiang, China

ARTICLE INFO

Article history:
Received 4 December 2024
Received in revised form
25 March 2025
Accepted 7 August 2025
Available online 12 August 2025

Edited by Teng Zhu and Xi Zhang

Keywords:
Plunger lift
Convolutional neural network
Abnormal condition diagnosis
Transfer learning
Gas well deliquification

ABSTRACT

Timely anomaly detection is critical for optimizing gas production in plunger lift systems, where equipment failures and operational issues can cause significant disruptions. This paper introduces a two-dimensional convolutional neural network (2D-CNN) model designed to diagnose abnormal operating conditions in gas wells utilizing plunger lift technology. The model was trained using an extensive dataset comprising casing and tubing pressure measurements gathered from multiple wells experiencing both normal and anomalous operations. Input data underwent a rigorous preprocessing pipeline involving cleaning, ratio calculation, window segmentation, and matrix transformation. Employing separate pre-training and transfer learning methods, the model's efficacy was validated through stringent testing on new, previously unseen field data. Results demonstrate the model's acceptable performance and strong diagnostic capabilities on this novel data from various wells within the operational block. This confirms its potential to fulfill practical field requirements by offering guidance for adjusting production systems in plunger lift-assisted wells. Ultimately, this data-driven, automated diagnostic approach provides valuable theoretical insights and technical support for sustaining gas well production rates.

© 2025 The Authors. Publishing services by Elsevier B.V. on behalf of KeAi Communications Co. Ltd. This is an open access article under the CC BY-NC-ND license (http://creativecommons.org/licenses/by-nc-nd/4.0/).

1. Introduction

As the process of natural gas extraction continues, the gas reservoir depletes, and with the gradual reduction of reservoir energy and bottomhole pressure, the production of the gas well steadily declines. Consequently, the kinetic energy of the gas is insufficient to lift the produced liquid to the surface, leading to liquid accumulation in the wellbore, forming liquid column and adding backpressure at the bottom of the wellbore (Lea and Rowlan, 2019; Luo et al., 2023; Wang et al., 2023b). The accumulated liquid is mostly a mixture of edge-bottom water (the major component) and gas condensate.

A significant challenge in natural gas well production is liquid loading, which occurs when accumulating liquids elevate bottomhole pressure, resulting in a rapid decrease in gas output. Plunger lift technology has become a prevalent deliquification strategy, designed to intermittently remove these liquids from the wellbore and restore standard production operations.

The deleterious effects of liquid accumulation on both the reservoir and wellbore are multifold. Firstly, the influx of produced water into high-permeability zones and fractures, driven by capillary and imbibition forces, acts as a significant barrier to gas flow, hindering efficient extraction of gas reservoir. Furthermore, the accumulated liquid significantly reduces the effective gas permeability due to relative permeability effects, leading to a precipitous decline in well production and an accelerated onset of the depletion stage, thereby compromising the ultimate gas field

* Corresponding author.
** Corresponding author.
E-mail addresses: jianjun-zhu@cup.edu.cn (J.-J. Zhu), haiwen-zhu@utulsa.edu (H.-W. Zhu).

Peer review under the responsibility of China University of Petroleum (Beijing).

https://doi.org/10.1016/j.petsci.2025.08.017
1995-8226/© 2025 The Authors. Publishing services by Elsevier B.V. on behalf of KeAi Communications Co. Ltd. This is an open access article under the CC BY-NC-ND license (http://creativecommons.org/licenses/by-nc-nd/4.0/).

recovery. The presence of water can exacerbate wellbore integrity issues through scaling and corrosion, potentially culminating in wellbore failure. The transition from single-phase gas flow to two-phase gas-liquid flow due to increased water production introduces significant flow resistance (Rastogi and Fan, 2020) and additional processing complexities (Zhao et al., 2021a, 2021b). Severe liquid accumulation can further render gas well inoperable through liquid loading (Karadkar et al., 2022; Tan et al., 2023), necessitating intervention techniques or even permanent abandonment (Jia et al., 2023). Finally, the presence of water not only diminishes the intrinsic value of the produced gas but also necessitates additional operational expenditures for dehydration processes, impacting overall economic viability.

Fig. 1(a) shows the liquid loading effect on the absolute open flow (AOF) of a typical gas well in China, with the deliquefaction technique of plunger lift (shown in Fig. 1(b)) used for production remediation. As seen, the AOF decreases significantly due to liquid production, which dominates the decline trend compared to other factors. Plunger lift uses only reservoir energy to cyclically unload accumulated liquids from the bottom of the wellbore, intermittently maintaining gas production. Thus, as Fig. 1(b) illustrates, the number of new wells equipped with plunger in that gas field has steadily increased, resulting in a stable increment of gas production over time.

A plunger is a free-traveling piston that fits within the production tubing and depends on well pressure to rise and solely on gravity to return to the bottom of the well (Lea and Rowlan, 2019). Fig. 2 demonstrates a typical plunger lift installation. As shown, plunger lift optimizes gas well production through a controlled cycle of liquid removal. An electrically actuated valve at the wellhead governs the process, allowing a free travel plunger within the wellbore to minimize liquid backflow and gas leakage. By acting as a distinct gas-liquid interface, the plunger leverages reservoir energy more effectively than traditional slug or bubble flow regimes. Compared to other artificial lift methods, plunger lift excels at removing liquids while preserving both reservoir energy and bottomhole pressure. This efficiency translates to extended production cycles for gas wells (Xing et al., 2025).

With the motor valve closed, gravity pulls the plunger through the wellhead catcher and down the tubing, first encountering gas, then liquid, and finally landing on the bumper spring. Casing pressure gradually rises; while tubing pressure spikes (Fig. 3), its rate of change is dictated by reservoir energy. The gap between tubing and plunger allows fluids above and below to communicate. Opening the motor valve connects the tubing to the surface pipeline, releasing gas pressure in both tubing and casing. The gas

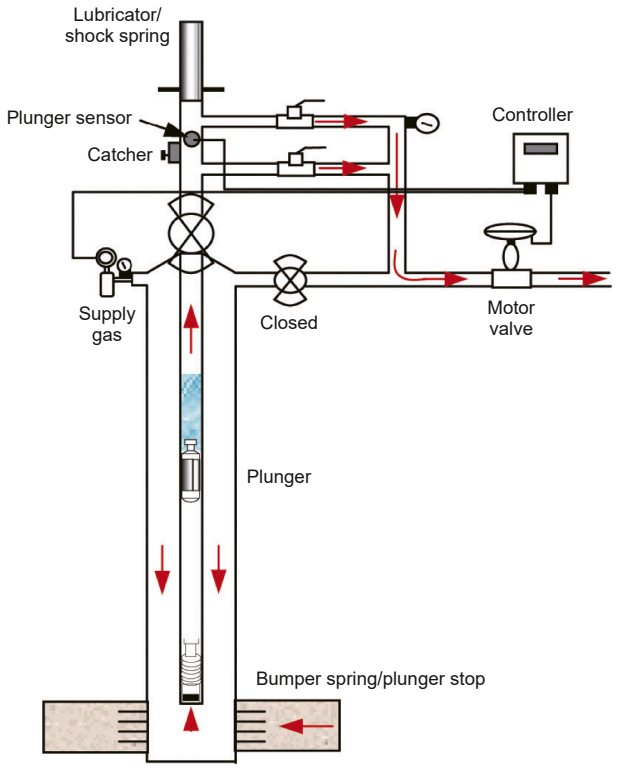

Fig. 2. Schematic of a typical plunger-lift installation (figure courtesy of petrowiki).

expansion propels the plunger and overlying liquid upward. Meanwhile, casing gas enters the tubing, causing both casing and tubing pressures to decline. Upon reaching the surface, the gas well resumes normal production. If bottomhole pressure and production rate fall significantly, the plunger cycle repeats.

For normal operations of plunger lift, several models have been studied in literature (Gupta et al., 2017; Zhao et al., 2021a, 2021b; Ye et al., 2022) to study the dynamic behaviors of plunger lift. Unlike normal operation, gas wells with plunger lift can experience various anomalies: liquid loading (Zhu et al., 2019), tubing rupture (Nguyen, 2020), stuck motor valves (Lea and Rowlan, 2019), and sudden pipeline pressure increase (Zhu et al., 2021). Liquid loading due to low gas velocity, especially in a large-diameter tubing, can rapidly fill the wellbore (Zaimes et al., 2019). Declined formation pressure reduces gas flow, shifting flow regimes from mist to slug/bubble flow and significantly

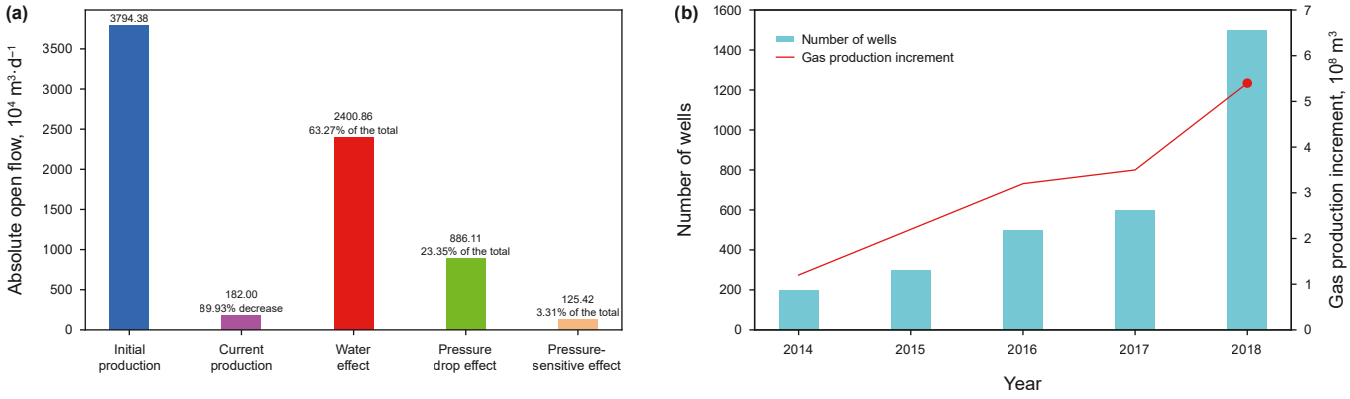

Fig. 1. Liquid loading and deliquification technique for a typical gas field in China (Cao et al., 2019): (**a**) liquid loading effects, (**b**) yearly plunger lift applications.

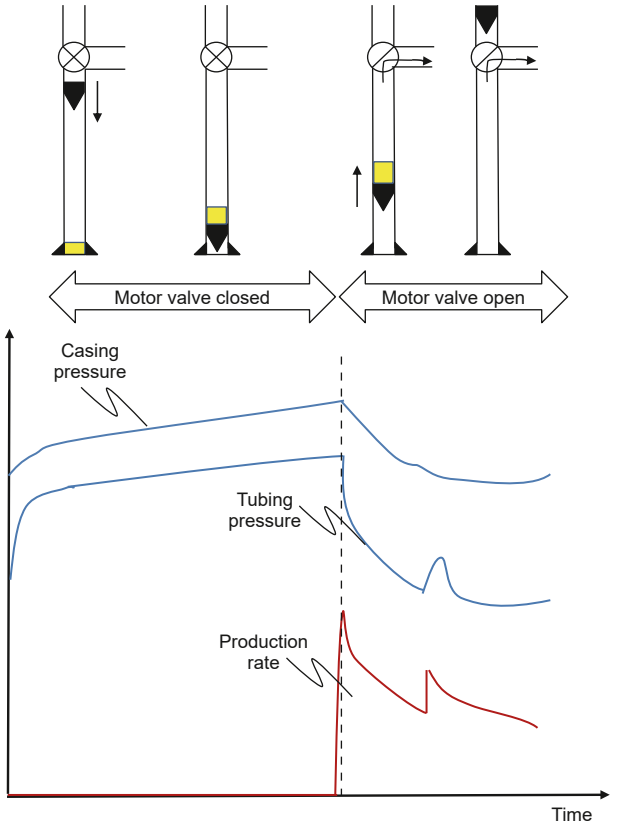

Fig. 3. Normal operation during single production cycle of plunger lift.

decreasing liquid carrying capacity, which can be detected through a clear departure of tubing and casing pressures.

Additionally, long-term production can cause casing fractures due to scaling, corrosion, or wear. During shut-in, tubing fractures allow liquid flow from casing to tubing, causing rapid casing pressure drop and tubing pressure rise. In extreme cases, tubing and casing pressures equalize, severely impacting production. Motor valve malfunctions further disrupt plunger lift operations (Shi et al., 2025). A stuck-open valve keeps the well continuously flowing, preventing pressure buildup for reservoir recovery. Conversely, a stuck-closed valve isolates the well, causing both tubing and casing pressures to gradually increase until the issue is effectively addressed (Agwu et al., 2024; Maut et al., 2024).

Fig. 4 illustrates the field production data for a typical plunger-lift-assisted gas well in southwestern China (Xie et al., 2023). In the figure, the upper curve represents the casing pressure, while the lower curve corresponds to the tubing pressure. According to the expertise of subject matter experts (SMEs), four distinct operational conditions, i.e., early/late liquid loading, liquid unloading, abnormal production, can be recognized. While analyzing production data for plunger-lift gas wells might seem straightforward, manually identifying anomalies across thousands of wells is impractical. Worse, a universally validated and comprehensive troubleshooting method for plunger lift anomalies remains elusive (Xie et al., 2023; Shi et al., 2025).

With the booming of Artificial Intelligence (AI) featured by Machine Learning (ML) algorithms and big data, the oil and gas industry are witnessing a surge in AI technologies and applications (Kuang et al., 2021; Niggemann et al., 2021). From subsurface studies and exploration to drilling, production, reservoir studies, and transportation, AI and ML techniques prove instrumental in addressing numerous complex challenges (Zhong et al., 2024). Among these, drilling and production emerge as focal points of research, marked by a wealth of available literature (Choubey and Karmakar, 2021). As to plunger lift data analytics, Kamari et al. (2017) developed a predictive model using a least squares support vector machine (LSSVM) approach to calculate the maximum possible liquid production rate for plunger lift systems. Trained on a robust dataset of literature-derived maximum rate, depth, tubing size, etc., the LSSVM model achieved a high coefficient of determination (R^2 = 0.929), indicating strong correlation and facilitating improved simulation and petroleum-production management.

Singh (2017) demonstrated the application of CART models for root cause analysis and production diagnostics in plunger lift systems, using field data to rank performance, troubleshoot issues (e.g., buildup times, plunger velocity), and guide operational improvements. Later, Singh et al. (2022) presented an integrated ML framework employing PCA, regression trees, and contribution

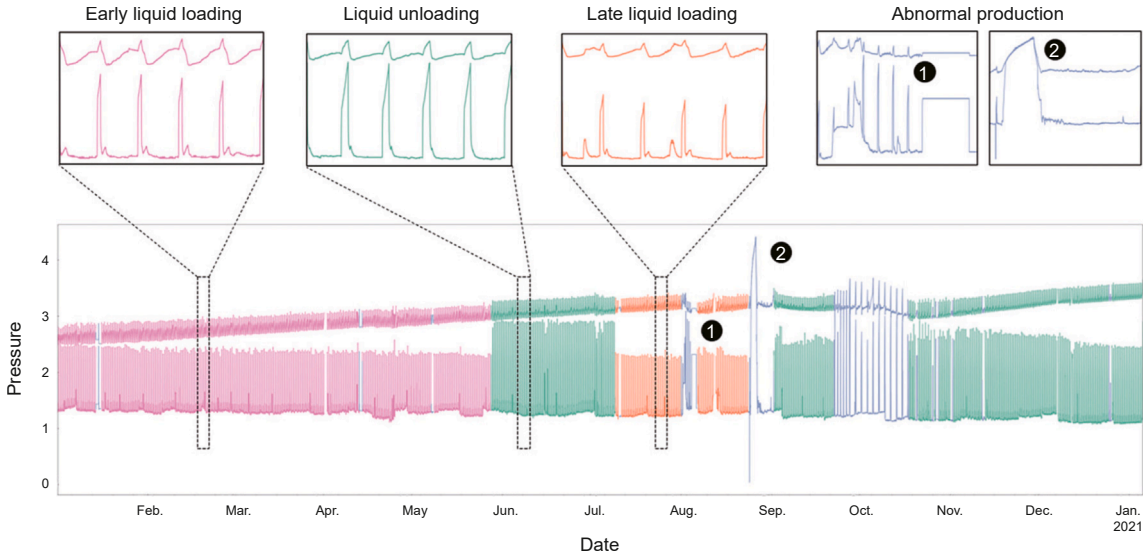

Fig. 4. Typical field data for a plunger-lift-assisted gas well (Xie et al., 2023).

charts for efficient monitoring and diagnostics. This cloud-based system, accessible via various interfaces, automates anomaly detection, simplifies diagnostics, and identifies key production drivers across many wells. Validation confirmed its effectiveness in trend analysis, well categorization, and root cause identification, highlighting its value for optimizing production.

Barros et al. (2018) introduced an innovative automated optimization method for plunger lift systems in unconventional shale wells. The authors developed diagnostic algorithms based on statistical analysis to automatically identify issues like irregular cycles, which were integrated into the SCADA system for real-time well diagnostics, leading to a 10% improvement in production potential and a reduction of undetected leaks by 600 bbl/d after one year. The approach also unveiled previously unknown optimal operating envelopes, significantly reducing manual efforts, and enhancing economic outcomes.

Akhiiartdinov et al. (2020) proposed a machine learning approach to optimize plunger-lifted well operation by simulating gas production and identifying optimal valve opening/closing times. The models, trained on field data, achieve acceptable accuracy and lead to a 23.8% increase in gas production compared to traditional methods. This data-driven approach offers real-time optimization and flow rate allocation capabilities, making it a valuable tool for the oil and gas industry.

Due to changing conditions and low data quality of gas wells, to optimize gas-assisted plunger lift (GAPL) or plunger-assisted gas lift (PAGL) is quite challenging. Hingerl et al. (2020) developed a plunger lift optimization software incorporating a novel physics engine for downhole insights, dynamic well optimization for anomaly detection, and artificial intelligence for continuous set-point optimization. The methodology aims to enhance plunger lift surveillance and control at scale, potentially increasing well stability, production rates, and operational efficiency.

For automatic optimization using machine learning, Romero et al. (2021) created a neural network to classify plunger lift failures and detect production losses. Trained on images converted from head pressure data, the model reached 80% accuracy on new failures, helping target optimization efforts. Separately, Shi et al. (2025) developed a sophisticated WT-MACNN model for diagnosing plunger gas lift system failures. Achieving over 83% accuracy in test and field conditions, their model surpassed traditional ML methods, providing an effective real-time diagnostic tool.

Our prior contributions include simulation-based and machine learning approaches to plunger lift diagnostics. Zhu et al. (2019, 2021) performed production diagnosis using transient simulations grounded in first-principle models, analyzing field data signatures and generating synthetic failure scenarios to understand root causes. Separately, Xie et al. (2023) developed an unsupervised deep clustering method to circumvent costly data labeling. Using a transformer encoder for identifying periodic points and partitioning data, this study found deep autoencoders achieved high clustering accuracy through compact representations. Furthermore, the cyclic-feature-based algorithm proved superior to sliding windows for clustering input data, offering a cost-effective way to analyze large datasets for performance optimization.

While significant progress has been made in optimizing plunger lift systems and their supporting devices, effectively identifying and resolving abnormal operating conditions remains a key challenge. Field-collected production data offers a promising avenue to address this gap. By analyzing features like pressure and flow rates during abnormal periods, data-driven diagnostic models can be constructed to pinpoint potential system faults accurately. This capability enables informed, targeted adjustments and optimizations, thereby enhancing the overall operational efficiency and reliability of plunger lift systems.

2. Methodology

By analyzing a large amount of plunger lift field data, the goal is to study the data characteristics for anomaly detection. The dataset is labeled by Subject Matter Experts (SMEs) and further processed to enhance input features. A 2D-CNN model is built for anomaly diagnosis. The pressure data and diagnosis results are integrated and displayed to optimize the plunger lift system operations.

2.1. Data preparation

Similar to our prior research (Xie et al., 2023), the source of the field data in this study is four natural gas wells (denoted as Wells 1–4) equipped with plunger lift systems, located in Chongqing, southwestern China. The complete dataset comprises various wellhead sensor signals, including tubing pressure, casing pressure, line pressure, and instantaneous production, as shown in Fig. 5. Spanned from Jan. 2020 to Apr. 2021, consisting of over 680,000 sets of minute-level production data of plunger lift, the dataset was preprocessed to better fit the model training and testing. The original data, depicted by the red dashed circles in Fig. 5, contains gaps and inconsistencies due to missing values or sensor malfunctions, which necessitates further feature engineering to handle these issues and prepare the data for analysis.

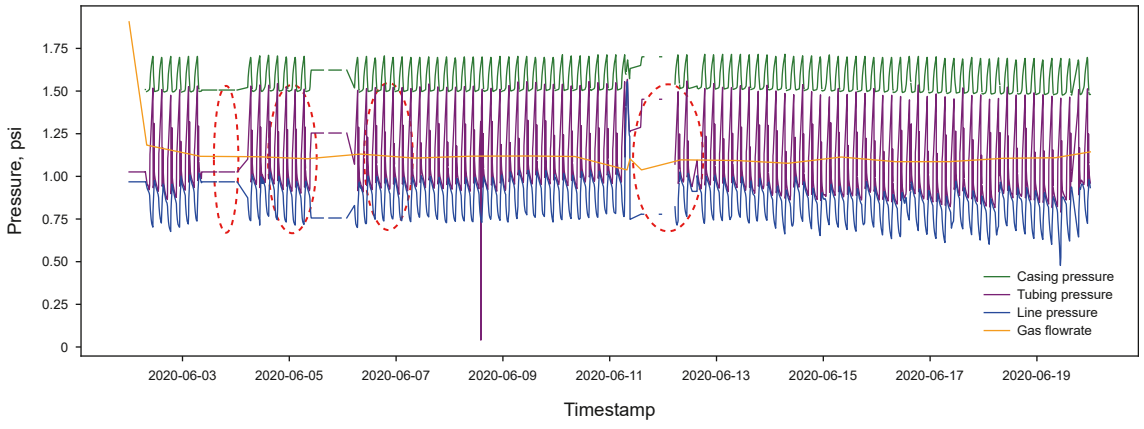

Fig. 5. Original field data sample for plunger-lift-assisted gas well.

Table 1
Typical operational conditions and labels of plunger lift.

Label	Anomaly type	Description	Typical pressure feature
0	Normal	Tubing/casing pressure change periorically and normally	
1	Motor valve won't open	Valve closing maintaine stable increase of tubing and casing pressures for an extended period	
2	Motor valve won't close	Valve opening connects tubing with surface pipeline, leading to gradual liquid buildup in the gas well and a slow, steady rise in casing pressure	
3	Unreasonable open/close periods	Unreasonable cyclic open/close induce wellbore liquid loading, causing oil and casing pressure to diverge noticeably over time	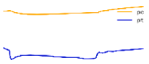
4	Other anomalies	Non-instrumental anomalies induce erratic tubing and casing pressure behavior, complicating production predictability	
5	Sensor malfunction	Field sensor disconnection or malfunction lead to data recording problems, resulting in fixed tubing and casing pressure readings for an extended duration	

* The yellow curve represents the casing pressure, while the blue curve represents the tubing pressure.

Initial examination of the raw data revealed that only tubing and casing pressure were suitable for anomaly detection in plunger lift applications due to limitations in other sensor data. Missing values in the gas well dataset were handled through linear interpolation, utilizing data points from the immediate minute before and after the gap. Duplicate pressure readings were identified and removed, keeping only the first instance of each value. After data cleaning and featuring, several operational conditions and corresponding labels of plunger lift can be obtained by SMEs, as listed in Table 1.

The operational cycle of a plunger lift system, fully outlined by the curve variations in Table 1, involves dynamic pressure changes closely tied to valve actions and fluid movement. This cycle is typically divided into four stages based on the plunger's motion and distinct pressure signatures: upward travel, afterflow, downward travel, and recovery. The first stage, upward travel, begins as expanding gas below the plunger lifts it; this action draws casing gas into the tubing, reducing both pressures. The reduction occurs because the expanding gas displaces the overlying liquid, lessening the tubing's hydrostatic head. The stage concludes when the plunger surfaces, discharging the liquid slug, which manifests as a sharp rise in tubing pressure as gas production commences.

Continued production leads to liquid re-accumulation and increased backpressure at the well base, causing casing pressure to rise and tubing pressure to fall. The plunger then descends under gravity, a phase typically marked by stable casing pressure due to negligible gas flow. In the subsequent shut-in (recovery) phase, casing pressure stabilizes or slightly drops, balanced by reservoir inflow, while tubing pressure rebuilds as the reservoir replenishes fluids. Once the wellbore pressure reaches a target level, the recovery stage ends, and the system prepares for the next cycle.

Due to the inherent variability of field data and unreliable valve sensors for signaling open/close statuses, accurately segmenting plunger lift data into distinct production cycles is challenging. To address data segmentation issue and meet the input size requirement of the downstream CNN-based model, we employ a moving window approach (Fig. 6) in this study. As illustrated in Fig. 6, a window size of 200 min and step size of 40 min is chosen, allowing for extraction of preliminary data segments of (200, 2) dimensions (Yu et al., 2024).

Our dataset captures pressure fluctuations tied to operations such as liquid loading, unloading, and plunger cycles. Using a window size of 200 min allows each segment to encompass sufficient temporal data to represent these processes accurately. While smaller windows might provide more granular detail, they can lead to higher computational costs and greater sensitivity to noise. Conversely, larger windows may smooth out critical transient features. A 200-min window size strikes a balance, achieving strong model accuracy and interpretability as confirmed through cross-validation experiments.

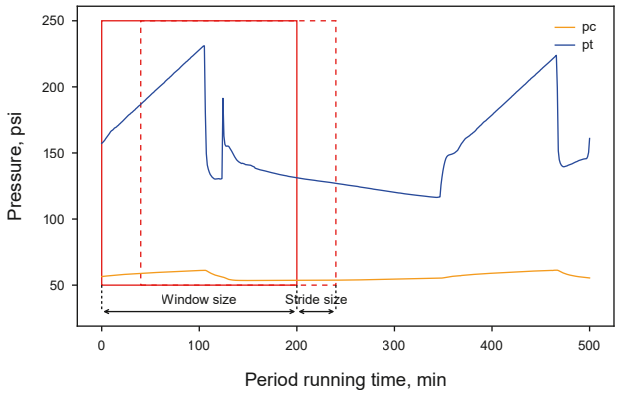

Fig. 6. Moving window technique for time-series data segmentation.

To maintain temporal continuity, a step size of 40 min ensures an 80% overlap (160 min) between adjacent windows. This overlap helps capture gradual changes in pressure trends without introducing excessive redundancy. Smaller step sizes, such as 20 min, result in too much overlap and unnecessary computational overhead, while larger steps risk losing important contextual information. A 40-min step effectively preserves pattern continuity and efficiency.

Within each window, pressure variations were visualized, and operational conditions were manually labeled based on the characteristic patterns of plunger lift. Given 6-class labels (0–5), employing one-hot encoding to transform them into categorical features is a common practice in machine learning (Chen et al., 2024). This enhances the model's ability to understand relationships between classes and potentially leads to better classification performance.

2.2. Data visualization and augmentation

Data normalization is crucial for making features comparable and enabling effective model learning, typically achieved by scaling data to eliminate scale influences (Wang et al., 2023a). Standard methods like Min-Max or Z-score normalization struggle with plunger lift pressure data because pressure amplitudes vary widely between wells and over time. This data instability limits the applicability of conventional normalization, especially for new field data. Consequently, this study proposes a novel ratio-based approach that serves as both transformation and normalization. It calculates ratios using the current minute's processed pressures relative to the previous minute's values:

$$x_i' = \frac{x_i}{x_{i-1}} \tag{1}$$

where x_i and x_{i-1} correspond to ith and (i–1)th pressures, x_i' denotes the ith computed ratio.

The ratio-based method focuses on the relative changes between consecutive data points rather than relying on absolute values. By emphasizing how the current value compares to the previous one, this approach better captures the system's dynamic behavior, especially under fluctuating pressure conditions. As a result, it reduces the instability in the sample data and improves data comparability.

In practical field applications, newly acquired data often exhibit different amplitude ranges from historical data. Traditional normalization techniques require recalculating distribution parameters (e.g., maximum, minimum, mean, standard deviation) for each new dataset, which can be cumbersome in real-time scenarios. In contrast, the ratio-based method does not depend on the overall data distribution. Instead, it only requires calculations between adjacent time points, making it more flexible and efficient when handling newly incoming data.

With original pressures replaced by the calculated pressure ratios, the new dataset remains 2-dimensional. To enhance compatibility with CNNs, we leverage Li et al. (2023) matrix conversion algorithm, which transforms data arrays into grayscale images, effectively increasing data dimensionality. Fig. 7 shows the detailed calculation flowchart. We first combine tubing and casing pressure ratios into an array X, where x represents casing pressure and y represents tubing pressure. Then, we calculate its mean μ_X and standard deviation σ_X. Applying Eq. (2) below to each element, the grayscale matrix G for model input can be obtained.

$$G_{i,j} = 255 \times \frac{x_i - \mu_X \times y_j}{2 \times \sigma_X} \tag{2}$$

where i is the index of array X, and j corresponds to the index of y_j. μ_X and σ_X are the mean and standard deviation of array X (combined from tubing and casing pressure ratios) respectively.

Converting the grayscale matrix into a visual image (like Fig. 8) allows us to observe clear feature differences between various operating conditions of plunger lift. As illustrated in Fig. 8, the distinct visual patterns in the grayscale images, corresponding to diverse plunger lift conditions, validate the effectiveness of such data conversion for classification tasks using CNN-based deep learning models.

Subsequent to preprocessing via ratio calculation, windowing, and matrix operations to enrich features, the dataset (Jan. 2020–Apr. 2021) was divided for training, validation, and testing, with the pre-trained model evaluated on the test set. Since different plunger lift conditions (normal operations, malfunctions, etc.) produce unique pressure patterns indicative of system status, we converted the pressure ratio data into grayscale images. This image-based representation enhances data expressiveness by utilizing spatial structure, making it well-suited for analysis by convolutional neural networks (CNNs).

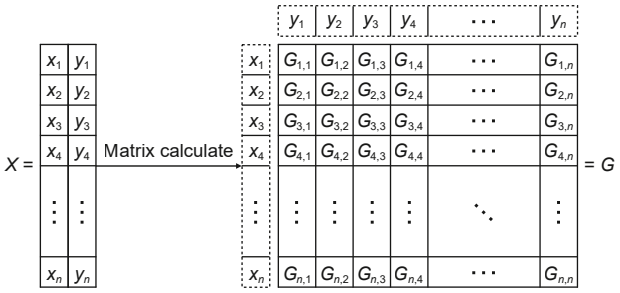

Fig. 7. Matrix conversion from data array to greyscale image.

CNNs are employed because they effectively extract local and global features from images, overcoming limitations in revealing complex relationships within raw, one-dimensional pressure data. Converting the pressure ratio data into 2D grayscale images preserves temporal information while introducing spatial correlations, making features more meaningful. This representation turns pressure fluctuations into distinct visual patterns (e.g., textures) that are easier to analyze than raw numbers. CNNs excel at classifying these visual features, detecting subtle and prominent differences between conditions. Consequently, this data transformation is crucial for enhancing compatibility with CNN models and enabling accurate classification of various operating states.

2.3. Model architecture

The anomaly detection model employs a 2D-CNN (built in TensorFlow) designed for 2D image input. The required input format is a 200 × 200 grayscale image (1 color channel). This resolution was chosen based on empirical testing comparing 100, 200, and 300-pixel images, where the 200-pixel format yielded consistently better results. A 200 × 200 resolution balances feature extraction capability with computational efficiency, preserving essential classification details without the information loss of lower resolutions or the excessive complexity and potential noise capture of higher resolutions. This optimal resolution aligns well with the data structure, facilitating accurate pattern learning.

Three convolutional layers extract local features via sliding filters, followed by three max pooling layers for dimensionality reduction and retaining key information. Four fully connected layers handle the large number of neurons, progressively reducing nodes until the final layer outputs the desired predictions. This architecture aims to extract meaningful features, reduce complexity, and provide an effective model, but its success hinges on proper hyperparameter tuning, training data, and validation. The schematic model architecture is presented in Fig. 9.

In the model, the convolutional and pooling layers utilize strides of (1,1), while convolution and pooling kernel sizes are set to (3,3) and (2,2), respectively. Same padding is chosen to preserve valid information, and the Dropout layer operates with a 0.2 drop rate. ReLU serves as the activation function for all non-output layers. The output layer uses the Softmax activation function to implement multi-class classification. A vector $\boldsymbol{S}$ containing n probability values (between 0 and 1) is output from forward calculation, indicating the input's likelihood for each working condition. The argmax function identifies the index of the element with the highest probability in $\boldsymbol{S}$, signifying the most likely working condition category for the input.

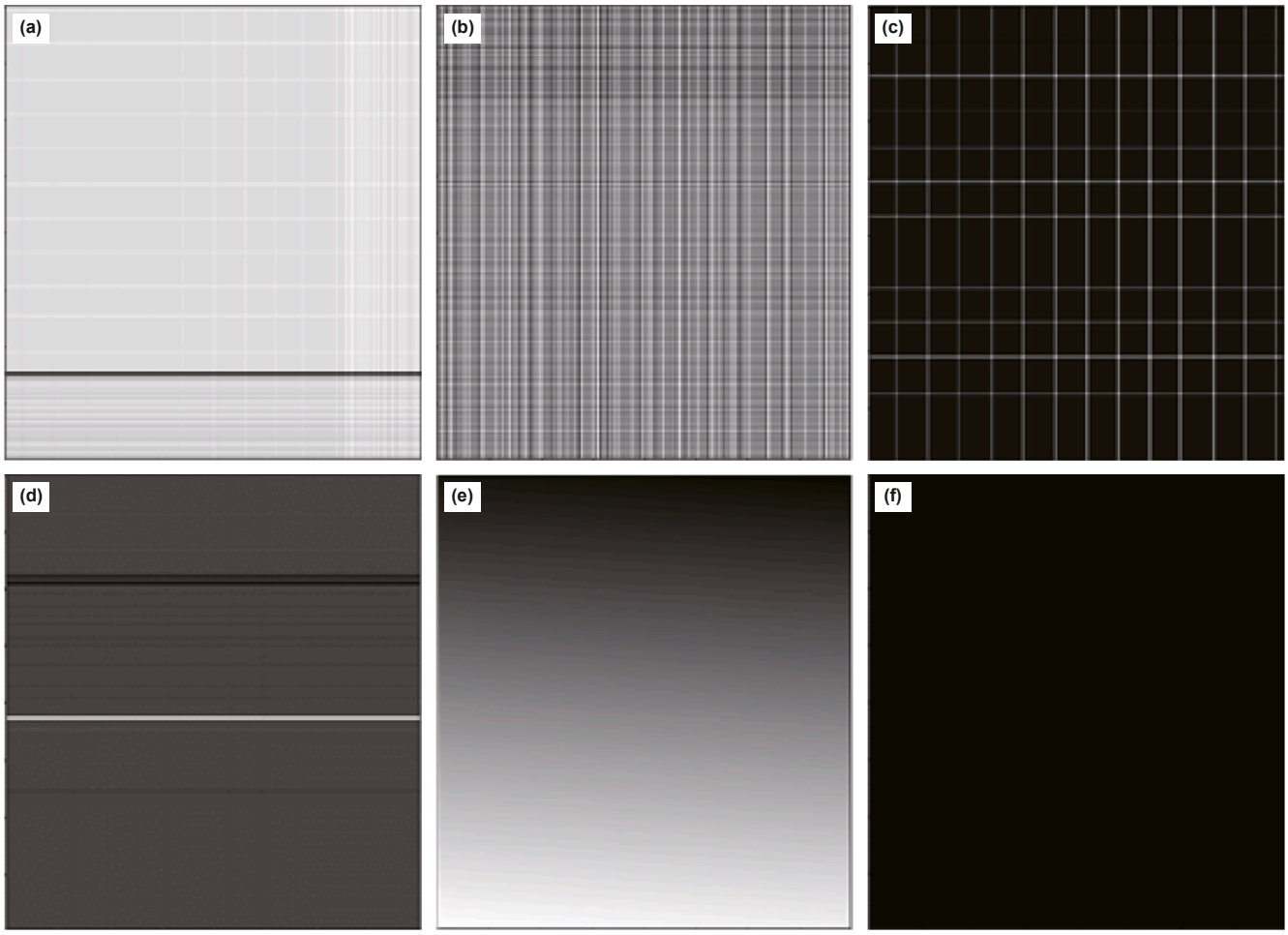

Fig. 8. Greyscale representation of plunger lift operational conditions: (**a**) normal condition, (**b**) valve abnormal close, (**c**) valve abnormal open, (**d**) unreasonable open/close, (**e**) other anomalies, (**f**) sensor malfunction (images obtained according to the matrix conversion illustrated in Fig. 7, where the *x*-axis represents the time steps (temporal dimension within each window) and the *y*-axis corresponds to the window index (spatial dimension across different windows).

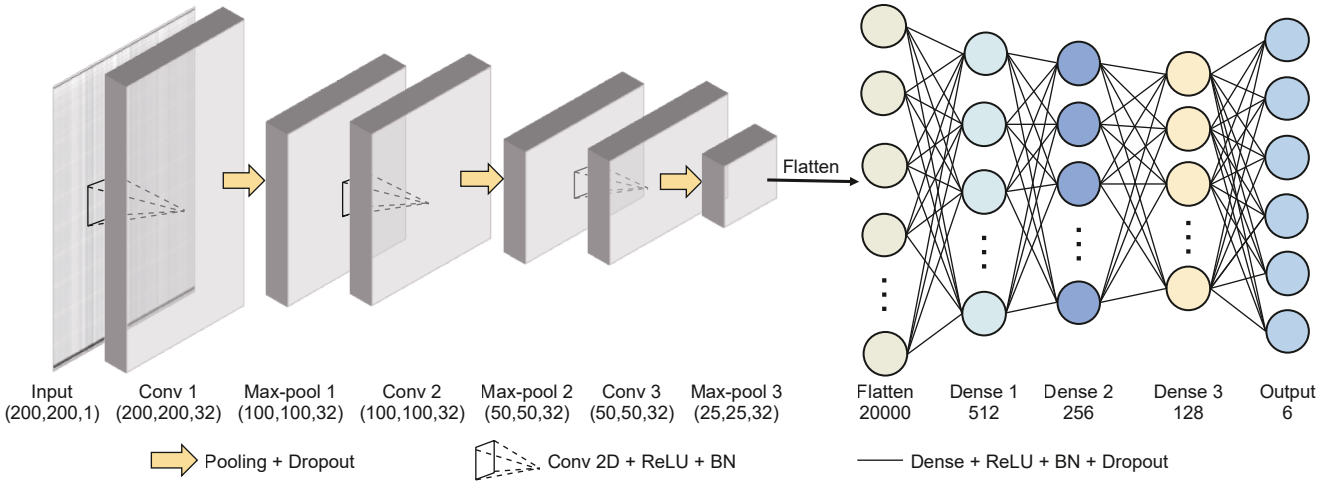

Fig. 9. CNN-based model architecture for anomaly detection of plunger lift.

2.4. Model training and evaluation

Deep learning models use loss functions to measure prediction error and guide parameter optimization towards higher accuracy. For the multi-class classification task of diagnosing plunger lift anomalies, the model utilizes a Softmax activation function in the output layer combined with the categorical cross-entropy loss function (Eq. (3)) to calculate the output error.

$$\text{loss} = -\sum_{i=1}^{n} y_i \cdot \log \widehat{y_i} \tag{3}$$

where n is the number of nodes in the output layer, y_i and $\widehat{y_i}$ are the values of the ith position in the one-hot encoding of the true label and the predicted label, respectively.

During training, Gradient Descent is a common method used to minimize the loss function, which represents the optimal solution identified through backpropagation. While aiming for fast model convergence, RMSprop is chosen as a specific optimization algorithm due to its advantages in adapting learning rates for individual parameters. The brief idea of RMSprop is given by:

$$S_{\mathrm{d}w} = \beta S_{\mathrm{d}w} + (1-\beta)\mathrm{d}w^2 \tag{4}$$

$$w = w - \alpha \frac{\mathrm{d}w}{\sqrt{S_{\mathrm{d}w}}} \tag{5}$$

where dw is the derivative of the weight w, $S_{\mathrm{d}w}$ is the gradient scaling factor, representing the weighted average of the gradients, α is the learning rate, β denotes the influence of past gradients on the current.

Post-training evaluation involves visualizing the training loss-accuracy curve, generating a confusion matrix for historical data tests, and calculating precision, recall, and F1 score for performance assessment. Due to six different classes in plunger lift conditions, the multi-class confusion matrix used in this study is listed in Table 2. The corresponding performance metrics for multi-class classification, i.e., precision, recall and F1 score are given by:

Table 2
Confusion matrix for anomaly detection of plunger lift.

True labels	Predicted labels					
	0	1	2	3	4	5
0	TP_{00}	E_{01}	E_{02}	E_{03}	E_{04}	E_{05}
1	E_{10}	TP_{11}	E_{12}	E_{13}	E_{14}	E_{15}
2	E_{20}	E_{21}	TP_{22}	E_{23}	E_{24}	E_{25}
3	E_{30}	E_{31}	E_{32}	TP_{33}	E_{34}	E_{35}
4	E_{40}	E_{41}	E_{42}	E_{43}	TP_{44}	E_{45}
5	E_{50}	E_{51}	E_{52}	E_{53}	E_{54}	TP_{55}

Table 3
Subsampling historical data of plunger lift production.

Labels	Samples before subsampling	Samples after subsampling			
		Total	Training	Validation	Testing
0	44,005	4401	2604	459	1338
1	2758	2758	1629	288	841
2	2056	2056	1239	218	599
3	9105	3035	1547	273	1215
4	3943	3943	2337	412	1194
5	3572	3572	2161	381	1030

$$\text{Precision} = \frac{\sum_{i=0}^{n} \frac{TP_{ii}}{TP_{ii} + \sum_j E_{ij}}}{n+1} \tag{6}$$

$$\text{Recall} = \frac{\sum_{i=0}^{n} \frac{TP_{ii}}{TP_{ii} + \sum_j E_{ji}}}{n+1} \tag{7}$$

$$\text{F1 score} = \frac{2\,PR}{P+R} \tag{8}$$

In above confusion matrix, E stands for “error”, representing misclassification cases. E_{ij} indicates the number of samples with true label i that were incorrectly predicted as class j. This is a 6×6 confusion matrix (6 classes from 0 to 5) showing the model's prediction performance for each class.

3. Results and discussion

This section evaluates the proposed CNN model's performance, highlighting the impact of the novel data augmentation technique. To improve generalization to unseen data, homogeneous transfer learning was employed. The effectiveness of the model's feature extraction throughout the training process is visualized using the t-SNE dimensionality reduction method.

3.1. Imbalanced data processing

For plunger-lift-assisted production, the prevalence of normal operation conditions leads to a historical data imbalance, where normal conditions heavily outnumber others. This skews training and risks models simply predicting “normal” for all inputs. To counteract this, we employed random subsampling technique with 70% of the data for training (including a 15% cross-validation subset), and 30% for testing.

Table 3 details the balanced distributions achieved before and after subsampling. The model was trained on the training subset, validated on the cross-validation subset, and its final performance evaluated on the independent test set. This approach ensures the model encounters a representative sample of all operational states, promoting effective training and mitigating biased predictions (see Table 4).

Initial model training used historical data (Jan. 2020–Apr. 2021) from four wells. To enhance generalizability, transfer learning was performed using unseen data (Apr.–Jun. 2022) from the same wells, which involved freezing all but the final layer of the pre-trained model (preserving architecture and initial weights) and fine-tuning its hyperparameters. This adapted the model's core knowledge to the new data. To address class imbalance in the Apr.–Jun. 2022 dataset, random subsampling was applied during transfer learning. Finally, the model performance was rigorously evaluated on an independent Jul.–Sep. 2022 dataset.

Table 4
Model performance by different types of data preparation.

Data preparation	Input size	Precision	Recall	F1 score
Raw data	(200, 2)	0.515	0.521	0.518
Matrix based on raw data	(200, 200, 1)	0.675	0.672	0.673
Matrix based on computed ratios	(200, 2000, 1)	0.806	0.804	0.803

3.2. Model performance on historical data

During pre-training, we evaluated the proposed ratio combined with matrix operation input format against two alternatives: (1) feeding cleaned raw data (200, 2) to a 1D CNN, and (2) applying matrix operations (Eq. (2)) to the raw data without ratio computation, thus using the resulting (200, 200, 1) data matrix and feeding it to a 2D CNN. As Table 3 reveals, the proposed method significantly outperformed both in terms of precision, recall, and F1 score, demonstrating superior performance.

As illustrated in Fig. 10, the model exhibits impressive training performance. The loss-accuracy curves indicate rapid convergence and good fitting (85% training, 80% validation accuracy) without signs of over/underfitting. The confusion matrix confirms strong anomaly detection capabilities, achieving high classification accuracy with a low false positive rate, meeting the pre-trained model's requirements. These results demonstrate the model's effectiveness for accurate anomaly detection, even with real-world data variability.

Fig. 11 displays sample model predictions against field data from the four wells, showing predicted condition labels alongside pressure readings. The model successfully classifies diverse operational conditions using tubing and casing pressures, demonstrating strong overall performance. While most anomalies are correctly identified with minimal false alarms, occasional misdetections occur, typically during brief, transient pressure fluctuations that complicate labeling (visible across wells in Fig. 11(a)–(d)). Despite these infrequent errors, the model reliably identifies condition changes, indicating satisfactory performance for handling varied operational scenarios.

3.3. Model performance with transfer learning

The model, initially trained on historical data, was further refined using transfer learning with new data from the same wells (Apr.–Jun. 2022) to improve feature extraction. The effectiveness of this process in separating data features was visualized using t-distributed stochastic neighbor embedding (t-SNE), a dimensionality reduction technique known for revealing patterns in high-dimensional data by preserving local structure in a low-dimensional representation (Xie et al., 2023).

t-SNE visualizations of key layer outputs (input, conv_2, dense_1, dense_3) illustrate the model's feature extraction capabilities on unseen data during transfer learning (Fig. 12). The plots show efficient feature learning, with increasing separation of data points representing different conditions as data progresses through the network layers. The clear clustering in the final dense layer indicates that highly discriminative features were learned, enabling the activation function to perform high-precision classification. This confirms the effectiveness of transfer learning in enhancing the model's anomaly detection performance.

Fig. 12 depicts the evolution of feature distributions visualized via t-SNE across selected model layers (input, conv_2, dense_1, dense_3), revealing the progressive refinement of feature extraction. Initially, at the input layer, the data points are scattered, reflecting the raw data's complexity and the difficulty of early-stage classification. Processing through the conv_2 layer induces initial clustering as local features are extracted; distinctions between conditions emerge, though feature separation remains incomplete due to some overlap.

Subsequent layers further enhance separability. In the dense_1 layer, clustering intensifies, and boundaries between conditions become clearer as features are integrated. This culminates in the dense_3 layer, where data points form distinct, concentrated clusters representing optimal separation among operating conditions, facilitating the model's highest classification accuracy. In summary, Fig. 12 demonstrates the model's systematic optimization of feature representation throughout its layers, transitioning from scattered input data to well-organized clusters, which underscores its strong feature extraction and classification capabilities for complex plunger lift scenarios.

The transfer learning model's performance was validated on completely unseen field data from Wells 1–4, covering Jul.–Sep. 2022 (Fig. 13). This real-world testing confirmed the model's effectiveness and potential for practical use, showing a high success rate in identifying anomalies and providing reliable classifications to guide system optimization. Performance varied slightly by well: Wells 1 and 2 showed generally accurate predictions with occasional errors during transient events; Well 3 was less consistent, suggesting a need for fine-tuning; and Well 4 performed moderately well but with some deviations. Despite these nuances, the model reliably identified most operating conditions across diverse scenarios.

The model's generalization capability and practical applicability were further validated through extensive testing on multiple gas wells within the block, using data from the Jul.–Sep. 2022

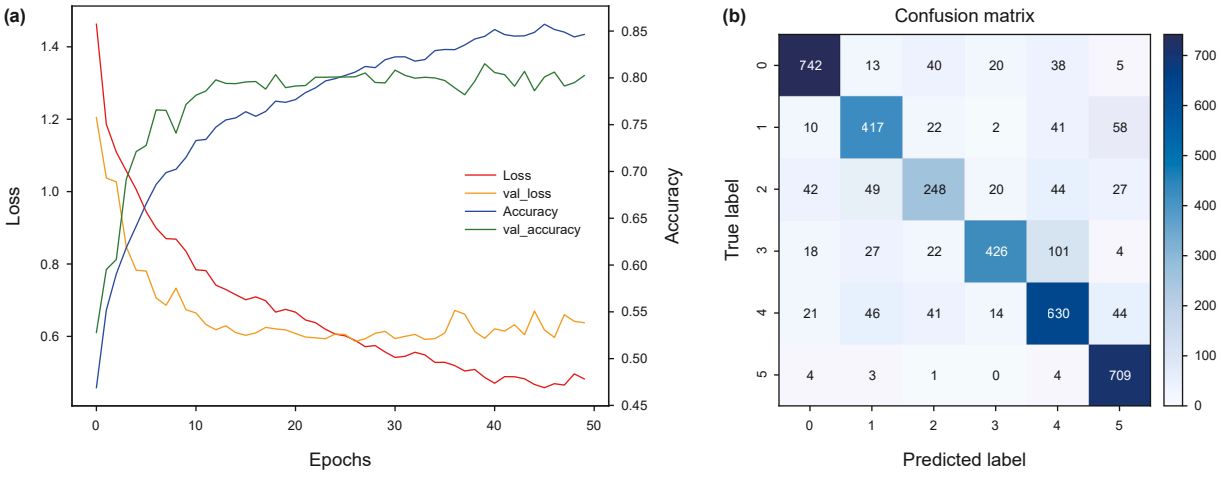

Fig. 10. Model training and performance: (**a**) loss-accuracy curves, (**b**) confusion matrix.

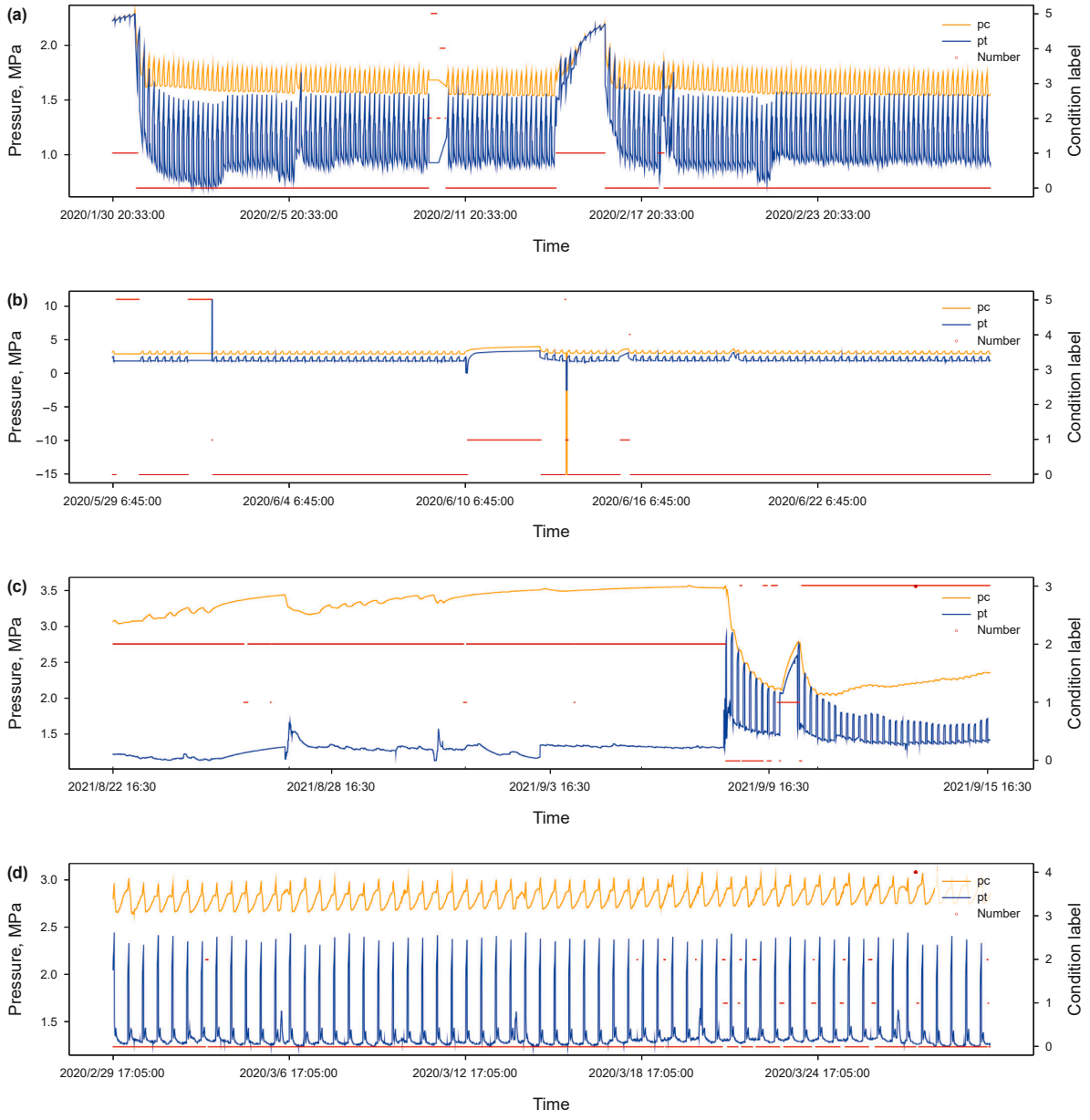

Fig. 11. Typical model predictions and corresponding field data: (**a**) Well 1, (**b**) Well 2, (**c**) Well 3, (**d**) Well 4.

period. Verification results for two additional wells (Well 5 and Well 6) are summarized in Table 5, with their performance visualized in Fig. 14. These examples illustrate generally satisfactory performance across the tested wells within the block. Fig. 14 shows the model's prediction performance on Wells 5 and 6. In both cases (Fig. 14(a) for Well 5, Fig. 14(b) for Well 6), the model tracks pressure changes effectively and identifies the majority of operational conditions correctly. However, both wells exhibit occasional misclassifications, particularly during rapid pressure fluctuations or transient events, suggesting sensitivity to data complexity or unique well characteristics.

While these tests demonstrate the model's ability to adapt to new data and achieve satisfactory results across different wells, the misclassifications highlight areas for future improvement, potentially through expanded training datasets or well-specific fine-tuning. Importantly, this broader validation confirms the model's overall robust performance and reliability. Its demonstrated success in identifying diverse anomalies, including wellbore issues and those stemming from human operations, reinforces its practical value for deployment in real-world gas production scenarios.

4. Discussion and conclusions

This study demonstrates the significant potential of a CNN-based model for automating anomaly detection in plunger lift

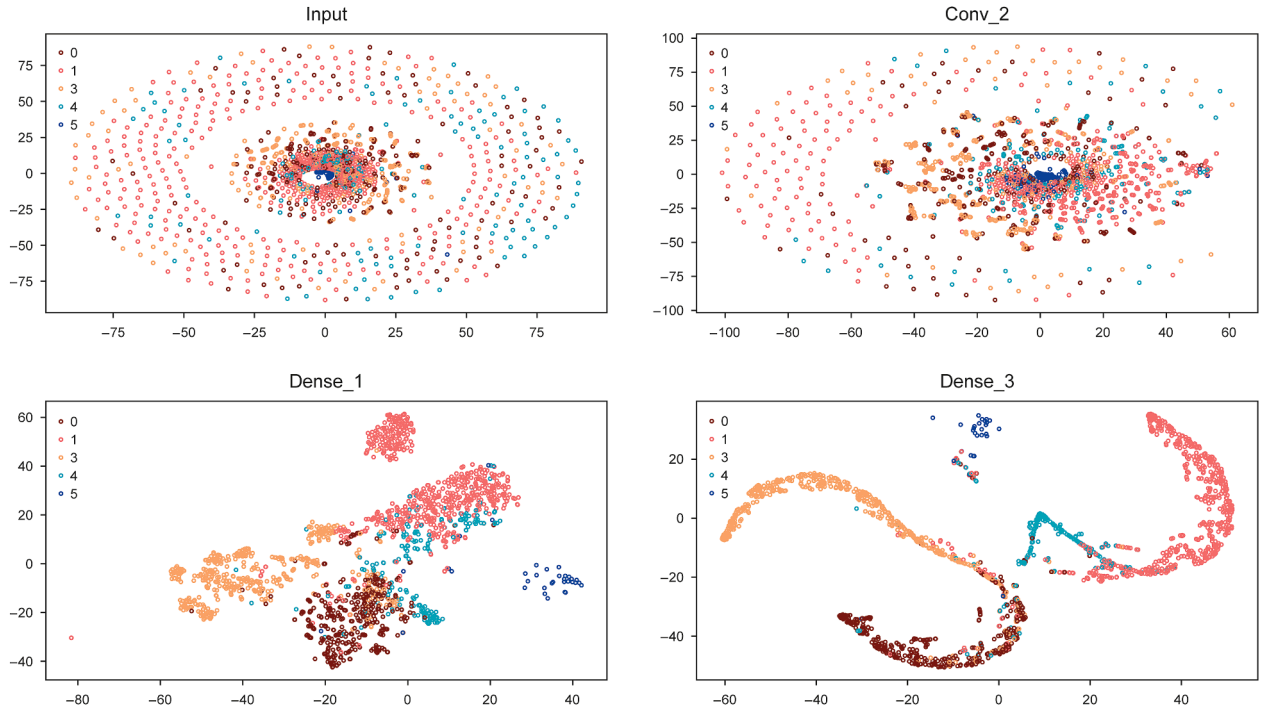

Fig. 12. *t*-SNE representation of the pretrained model during transfer learning based on the unseen dataset.

operations, representing a considerable advancement over manual diagnostic methods. However, certain limitations should be acknowledged. Firstly, data quality issues persist within the dataset (spanning over a year from four wells), including missing values, incomplete records often due to sensor failures, and variability in data distributions across wells. These factors may influence the model's generalization capability. Addressing these challenges through the collection of higher-quality historical data and further refinement of preprocessing techniques remains essential future work. Secondly, this study focused exclusively on tubing and casing pressure data. While critical, these variables alone do not capture the full complexity of production dynamics, which involve other parameters like temperature and flow rate. Future research incorporating these additional variables could provide a more comprehensive operational assessment, thereby enhancing the model's accuracy and robustness.

Despite these limitations, the developed model offers promising capabilities extending beyond simple anomaly detection to support production decision-making. By effectively classifying operational conditions, the model can furnish scientifically grounded recommendations, enabling operators to implement optimal strategies more rapidly, especially in complex scenarios. This dual function enhances the model's overall value for industrial applications.

In summary, this paper introduces an innovative automated anomaly detection approach for plunger lift systems, leveraging a CNN model enhanced by a novel data preparation technique involving ratio calculation and grayscale image conversion. This preparation method improves input data quality and significantly boosts the 2D-CNN model's performance. The key conclusions derived from this study are:

1. The proposed data preparation workflow (data cleaning, ratio calculation, window partitioning, matrix operations) yields grayscale matrices that effectively represent underlying data patterns and mitigate some inherent data quality issues.
2. This novel data preparation method significantly outperforms traditional approaches, as evidenced by improved performance metrics.
3. Employing transfer learning on a pretrained CNN model, specifically by retraining only the final fully connected layer, provides robust performance on unseen data while minimizing additional training costs.
4. Successful validation using data from different gas wells confirms the model's reliability in detecting anomalies, indicating its potential for broader application in optimizing plunger lift systems and reducing operational costs.
5. Identified limitations related to data quality and the scope of input variables underscore the need for advancements in sensor technology, expanded data collection, and the integration of additional parameters to further improve model robustness and production efficiency

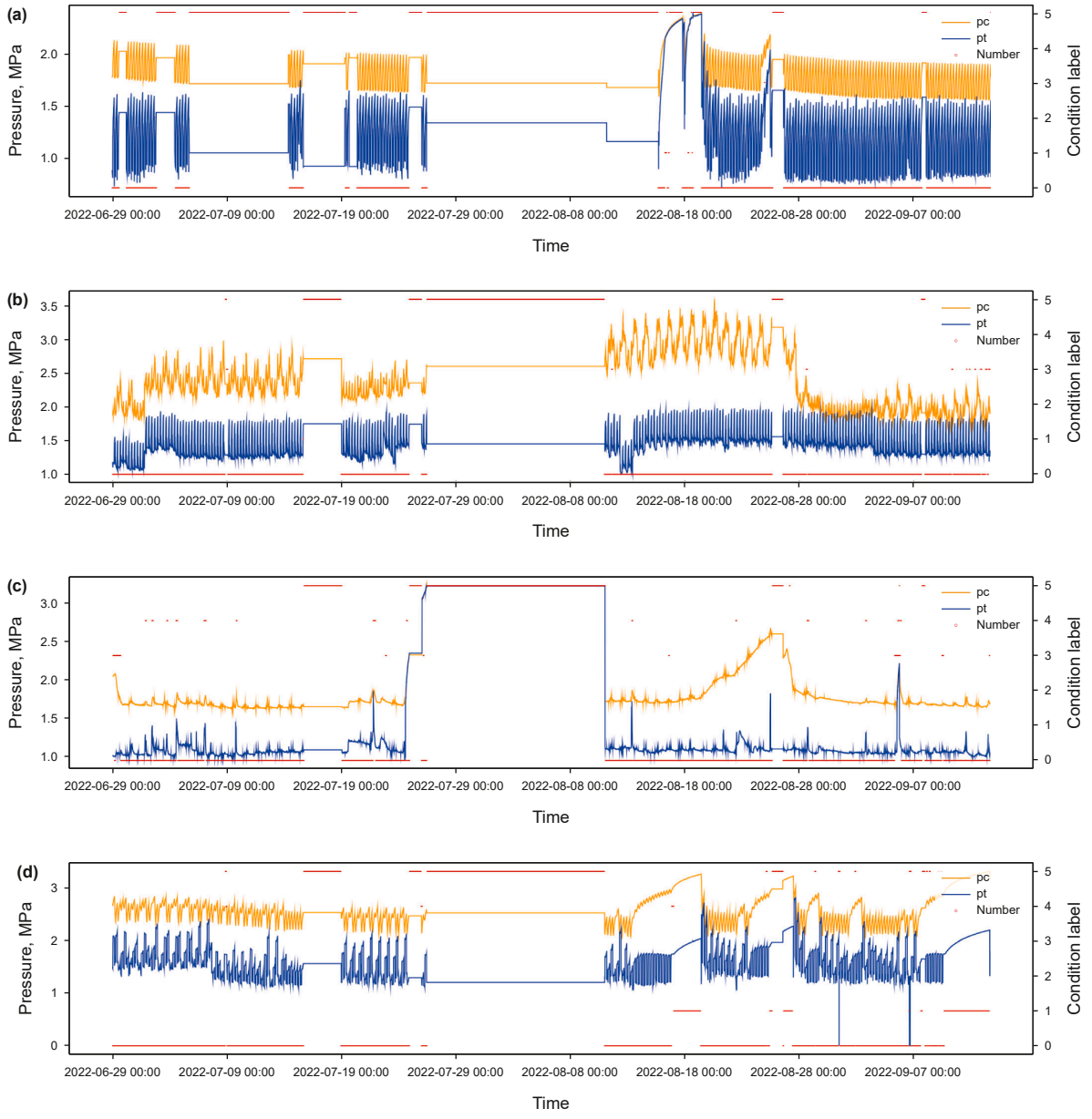

Fig. 13. Model performance by transfer learning on the unseen data: (**a**) Well 1, (**b**) Well 2, (**c**) Well 3, (**d**) Well 4.

Table 5
Model verification results on multiple gas wells.

Well ID	Precision	Recall	F1 score
Well 5	0.770	0.801	0.765
Well 6	0.732	0.836	0.779

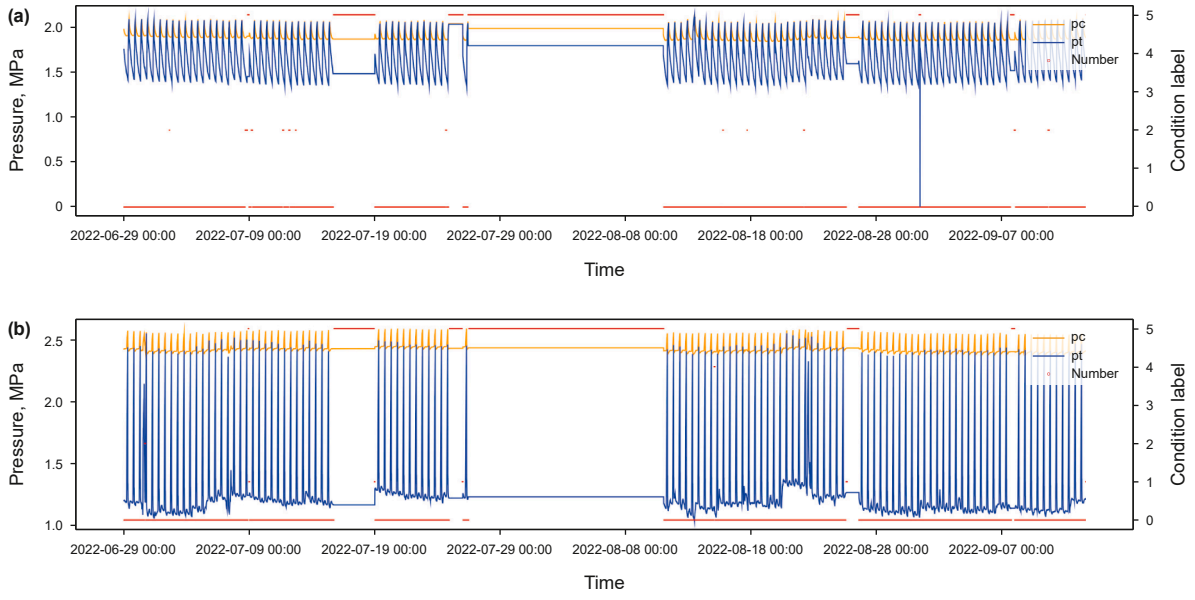

Fig. 14. Model performance by transfer learning on different wells from the same field, (**a**) Well 5, (**b**) Well 6.

CRediT authorship contribution statement

Qi-Xin Liu: Data curation, Methodology, Writing – original draft. **Jian-Jun Zhu:** Investigation, Project administration, Conceptualization. **Hai-Bo Wang:** Validation, Resources. **Shuo Chen:** Investigation, Validation, Data curation. **Hao-Yu Wang:** Visualization, Validation, Resources. **Nan Li:** Validation, Visualization, Resources. **Rui-Zhi Zhong:** Software, Investigation, Resources. **Hai-Wen Zhu:** Resources, Writing – review & editing.

Declaration of competing interest

The authors declare the following financial interests/personal relationships which may be considered as potential competing interests: Jianjun Zhu reports financial support was provided by National Natural Science Foundation of China. If there are other authors, they declare that they have no known competing financial interests or personal relationships that could have appeared to influence the work reported in this paper.

Acknowledgments

The authors would like to acknowledge the support of the National Natural Science Foundation of China (Grant No. 52474064), and Frontier Interdisciplinary Exploration Research Program of China University of Petroleum, Beijing (Grant No. 2462024XKQY005). The authors are grateful for the field production data of gas wells provided by PetroChina Research Institute of Petroleum Exploration & Development.

References

Agwu, O.E., Alatefi, S., Azim, R.A., Alkouh, A., 2024. Applications of artificial intelligence algorithms in artificial lift systems: a critical review. Flow Meas. Instrum., 102613 https://doi.org/10.1016/j.flowmeasinst.2022.102613.

Akhiiartdinov, A., Pereyra, E., Sarica, C., Severino, J., 2020. Data analytics application for conventional plunger lift modeling and optimization. In: SPE Artificial Lift Conference and Exhibition-Americas. OnePetro. https://doi.org/10.2118/201144-MS.

Barros, J.L., Claramunt, J.I., Ferrigno, E., 2018. Novel approach in digital diagnostic for plunger lift in unconventional Wells at Vaca Muerta. In: SPE Artificial Lift Conference and Exhibition - Americas, The Woodlands, Texas, USA. https://doi.org/10.2118/190930-MS.

Cao, G.Q., Jiang, X.H., Li, N., Jia, M., Zhang, Y., Wang, H.Y., 2019. Domestic and foreign research status and development direction of drainage gas recovery technologies in water-producing gasfields. Oil Drill. Prod. Technol 41, 614–623. https://doi.org/10.13639/j.odpt.2019.05.011. (in Chinese).

Chen, P.C., Li, R., Fu, K., Zhong, Z.K., Xie, J.L., Wang, J.L., Zhu, J.J., 2024. A cascaded deep learning approach for detecting pipeline defects via pretrained YOLOv5 and ViT models based on MFL data. Mech. Syst. Signal Process. 206, 110919. https://doi.org/10.1016/j.ymssp.2023.110919.

Choubey, S., Karmakar, G.P., 2021. Artificial intelligence techniques and their application in oil and gas industry. Artif. Intell. Rev. 54 (5), 3665–3683. https://doi.org/10.1007/s10462-020-09935-1.

Gupta, A., Kaisare, N.S., Nandola, N.N., 2017. Dynamic plunger lift model for deliquification of shale gas wells. Comput. Chem. Eng. 103, 81–90. https://doi.org/10.1016/j.compchemeng.2017.03.005.

Hingerl, F., Arnst, B., Cosby, D., Kreutzman, L., Tyree, R., 2020. The future of plunger lift control using artificial intelligence. In: SPE Artificial Lift Conference and Exhibition-Americas. https://doi.org/10.2118/201132-MS.

Jia, Y.L., Shi, S.Q., Tian, W., Tan, B., Yang, Y.C., Li, X.R., 2023. Transient modeling of plunger lift with check valve for gas well deliquification in horizontal well. Energy Sources, Part A Recovery, Util. Environ. Eff. 45 (1), 2267–2283. https://doi.org/10.1080/15567036.2023.2186540.

Kamari, A., Bahadori, A., Mohammadi, A.H., 2017. Prediction of maximum possible liquid rates produced from plunger lift by use of a rigorous modeling approach. SPE Prod. Oper. 32 (1), 7–11. https://doi.org/10.2118/180912-PA.

Karadkar, P., Alkhowaildi, M., Bulekbay, A., 2022. An innovative method to enable well kick-off and liquid unloading using dry ice. ADIPEC. https://doi.org/10.2118/211575-MS.

Kuang, L., He, L.I.U., Yili, R.E.N., Kai, L.U.O., Mingyu, S.H.I., Jian, S.U., Xin, L.I., 2021. Application and development trend of artificial intelligence in petroleum exploration and development. Petrol. Explor. Dev. 48 (1), 1–14. https://doi.org/10.1016/s1876-3804(21)60001-0.

Lea Jr, J.F., Rowlan, L., 2019. Gas Well Deliquification. Gulf Professional Publishing.

Li, G., Hu, J.Y., Shan, D.W., Ao, J., Huang, B., Huang, Z., 2023. A CNN model based on innovative expansion operation improving the fault diagnosis accuracy of drilling pump fluid end. Mech. Syst. Signal Process. 187, 109974. https://doi.org/10.1016/j.ymssp.2022.109974.

Luo, C., Gao, L., Liu, Y., Xie, C., Ye, C., Yang, J., Liu, Z., 2023. A modified model to predict liquid loading in horizontal gas wells. J. Energy Resour. Technol. 145 (8), 083502. https://doi.org/10.1115/1.4062504.

Maut, P.P., Prakash, Y., Dutta, U.A., Saikia, P.P., Sowmyanarayanan, N.M., Yadav, A., 2024. Plunger lift system: a field implementation case study in upper Assam Shelf Basin. In: APOGCE 2024, Perth, Australia. https://doi.org/10.2118/221173-MS.

Nguyen, T., 2020. Artificial lift methods. Petrol. Eng. https://doi.org/10.1016/b978-075068270-1/50074-8.

Niggemann, O., Diedrich, A., Kühnert, C., Pfannstiel, E., Schraven, J., 2021. A generic digitaltwin model for artificial intelligence applications. In: 2021 4th IEEE

International Conference on Industrial Cyber-Physical Systems (ICPS). Victoria, Canada, pp. 55–62. https://doi.org/10.1109/ICPS49255.2021.9468243.
Rastogi, A., Fan, Y., 2020. Experimental and modeling study of onset of liquid accumulation. J. Nat. Gas Sci. Eng. 73, 103064. https://doi.org/10.1016/j.jngse.2019.103064.
Romero, A., Feldmann, C., Alonso, K.S., Martinez, G., Barros, J., Montero, M., Ferrigno, E., 2021. Prescriptive model for automatic online plunger lift unconventional Wells optimization. In: Latin America Unconventional Resources Technology Conference, 16-18 November 2020. Unconventional Resources Technology Conference (URTEC), pp. 462–473. https://doi.org/10.15530/urtec-2020-1427.
Shi, H., Su, Y., Pan, Y., Zhang, W., Chen, Z., Liao, R., 2025. Research on failure diagnosis analysis of plunger gas lift system using convolutional neural network with multi-scale channel attention mechanism based on wavelet transform. Chem. Eng. Sci. 304, 121031. https://doi.org/10.1016/j.ces.2024.121031.
Singh, A., 2017. Application of data mining for quick root-cause identification and automated production diagnostic of gas wells with plunger lift. SPE Prod. Oper. 32 (3), 279–293. https://doi.org/10.2118/175564-PA.
Singh, A., Shukla, A., Purwar, S., 2022. Leveraging machine learning and interactive voice interface for automated production monitoring and diagnostic. In: SPE Annual Technical Conference and Exhibition. https://doi.org/10.1007/s13202-024-01777-9.
Tan, B., Liu, X., Liu, Y., Chang, Y., Tian, W., Jia, Y., Liang, X., 2023. Mechanism of liquid unloading by single flowing plunger lift in gas wells. Int. J. Hydrogen Energy 48 (7), 2571–2582. https://doi.org/10.1016/j.ijhydene.2022.10.118.
Wang, J., Ozbayoglu, E., Baldino, S., Liu, Y., Zheng, D., 2023a. Time series data analysis with recurrent neural network for early kick detection. In: Offshore Technology Conference. https://doi.org/10.4043/32428-MS.
Wang, X., Ma, W., Luo, W., Liao, R., 2023b. Drainage research of different tubing depth in the horizontal gas well based on laboratory experimental investigation and a new liquid-carrying model. Energies 16 (5), 2165. https://doi.org/10.3390/en16052165.
Xie, Y.K., Ma, S.F., Wang, H.Y., Li, N., Zhu, J.J., Wang, J.L., 2023. Unsupervised clustering for the anomaly diagnosis of plunger lift operations. Geoenergy Sci. Eng. 231, 212305. https://doi.org/10.1016/j.geoen.2023.212305.
Xing, Z., Han, G., Jia, Y., Tian, W., Gong, H., Zuo, H., Liang, X., 2025. Mechanistic modeling and experimental study of multistage plunger lift for liquid unloading in ultra-deep gas well. Geoenergy Sci. Eng. 246, 213653. https://doi.org/10.1016/j.geoen.2025.213653.
Ye, C., Tang, H., Cai, D., Xie, N., Wang, Q., Liu, J., Jiang, L., 2022. Research on the inflow performance of the plunger lift in the shale gas horizontal well. Math. Probl Eng. 2022, 4401128. https://doi.org/10.1155/2022/4401128.
Yu, D., Guo, G., Wang, D., Zhang, H., Li, B., Xu, G., Deng, S., 2024. Modeling dynamic spatio-temporal correlations and transitions with time window partitioning for traffic flow prediction. Expert Syst. Appl. 252, 124187. https://doi.org/10.1016/j.eswa.2024.124187.
Zaimes, G.G., Littlefield, J.A., Augustine, D.J., Cooney, G., Schwietzke, S., George, F.C., Skone, T.J., 2019. Characterizing regional methane emissions from natural gas liquid unloading. Environ. Sci. Technol. 53 (8), 4619–4629. https://doi.org/10.1021/acs.est.8b05546.
Zhao, K., Mu, L., Tian, W., Bai, B., 2021. Gas-liquid flow seal in the smooth annulus during plunger lifting process in gas wells. J. Nat. Gas Sci. Eng. 95, 104195. https://doi.org/10.1016/j.jngse.2021.104195.
Zhao, Q., Zhu, J.J., Cao, G.Q., Zhu, H., Zhang, H.Q., 2021. Transient modeling of plunger lift for gas well deliquification. SPE J. 26 (5), 2928–2947. https://doi.org/10.2118/205386-PA.
Zhu, J.J., Cao, G.Q., Tian, W., Zhao, Q., Zhu, H., Song, J., Zhang, H.Q., 2019. Improved data mining for production diagnosis of gas wells with plunger lift through dynamic simulations. In: SPE Annual Technical Conference and Exhibition. https://doi.org/10.2118/196201-MS.
Zhu, J.J., Jia, H., Wang, H.Y., Cao, G.Q., Zhu, H., 2021. Modeling and applications of plunger lift for gas well deliquification via a transient multiphase simulator. Pet. Sci. Bulletin 4, 626–637. https://10.3969/j.issn.2096-1693.2020.04.044. (in Chinese).
Zhong, Z.K., Wang, H.Y., Li, N., Zhu, H., Zhu, J.J., Wang, J.L., 2024. Prediction of plunger lift dynamics using a bidirectional long short-term memory neural network with an innovative forecasting strategy. In: 2024 IEEE 3rd International Conference on Electrical Engineering, Big Data and Algorithms (EEBDA). IEEE, pp. 80–85. https://doi.org/10.1109/eebda60612.2024.10485764.